Chalcogenide Letters Vol. 11, No. 2, February 2014, p. 79 - 90

STRUCTURAL, OPTICAL AND ELECTRICAL PROPERTIES OF ZnS NANOPARTICLES AFFECTING BY ORGANIC COATING

N. SOLTANI[a,*], A. DEHZANGI[b], A. KHARAZMI[a], E. SAION[a], W. MAHMOOD MAT YUNUS[a], B. YEOP MAJLIS[b], M. REZA ZARE[c,d], E. GHARIBSHAHI[a], N. KHALILZADEH[a]

[a]*Department of Physics, Faculty of Science, University Putra Malaysia, 43400UPM Serdang, Selangor, Malaysia*

[b]*Institute of Microengineering and Nanoelectronics (IMEN), Universiti Kebangsaan Malaysia, 43600 Bangi, Selangor, Malaysia*

[c]*Department of Electrical and Electronic, Faculty of Engineering, University Putra Malaysia, 43400UPM Serdang, Selangor, Malaysia*

[d]*Islamic Azad University, Majlesi Branch, Iran*

In this study the influence of the organic polymeric coating and its concentration on the structural, optical and electrical properties of ZnS nanocrystals has been investigated. In this matter, PVP-capped ZnS nanocrystals were prepared by a simple, rapid and energy efficient microwave method. The XRD results confirmed the formation of single phase cubic nanocrystalline structure. TEM images showed the formation of well isolated spherical nanoparticles with the average size of less than 5.5 nm. The presence of tensile strain in all samples was determined from Williamson-Hall analysis. The elemental compositions of Zn, S and O were quantitatively obtained from EDX analysis, where the FT-IR spectra confirmed coordination with O atoms of PVP. The band gap and absorption edge shift was determined using UV–visible spectroscopy. The PL spectra of the PVP-capped ZnS nanoparticles appeared broadened from 370 to 500 nm due to the presence of multiple emission bands attribute to the sulfur and zinc vacancies or compounded effect of PVP. The electrical property study of samples indicated the conductivity enhancement from 2.981×10^{-6} to 7.014×10^{-6} S/m by increasing PVP concentration. Increasing of dielectric constant and decrease in the peak value of tan δ by raising the PVP concentration were observed.

(Received November 17, 2013; Accepted February 25, 2014)

Keywords: ZnS nanoparticles, PVP, Williamson-Hall analysis, Photoluminescence, AC and DC conductivity, Dielectric constant

1. Introduction

Semiconductor nanomaterials, including II-VI binary compounds, have attracted tremendous attention due to their intriguing properties arising from the size quantization and extremely high surface to volume ratio of these materials which offer major advantages over their bulk materials. These nanoscale materials are expected to have many potential applications both in mesoscopic research electronics and development of nanodevices [1-4].

One of the most important II–VI semiconductors is ZnS nanoparticles with the direct wide band gap energy of 3.68 eV. Recently, for ZnS nanoparticles, several potential and actual applications were reported, i.e. in optoelectronic devices, light emitting displays, photocatalysis, solar cells and luminescent materials [3-6]. Many of these applications require nanostructures with the high dispersion, stability and size uniformity. In this matter, promising results have been achieved by coating of nanoparticles using organic materials such as polymers. Polymers can interact with

*Corresponding author: nayereh.soltani@gmail.com

the metal ions in the nanoparticles' surface by complex or ion-pair formation, which can be controlled or designed in order to vary the certain physical properties of nanaoparticles [7]. Surface capping of nanoparticles with polymers gives rise to have the structures with enhanced thermal stability, and reduced reactivity and agglomeration tendency [8-10].

Among the various methods for the preparation of polymer capped ZnS nanoparticles, microwave irradiation route is an effective preparation technique. This technique can provide homogenous internal and volumetric heating at rapid rates through the interaction of dipole moments or molecular ionics with electric or magnetic fields. Moreover, the microwave irradiation technique is capable of producing smaller particles in a size of few nanometers with a narrow particle size distribution and high purity with fast processing at low costs [1]. We already investigated the influence of microwave irradiation time on the optical and electrical properties of ZnS nanoparticles synthesized by polyol method [11]. Here, we intend to study how the presence of a commonly used organic polymeric coating and concentration affects ZnS nanoparticles' structural and physical behavior.

In this work, a simple microwave irradiation method was used for the synthesis of the polyvinyl pyrrolidone (PVP)-capped ZnS nanoparticles. Then the influence of PVP coating and concentration on the structural, optical and electrical properties of ZnS nanoparticles were studied in details using several techniques. The diversities of polymer capped nanoparticle properties with bare nanoparticles were explained on the basis of the structure, size and surface defects, along with the specific physicochemical interactions in the interphase region of the ZnS nanostructures and the polymer shell.

2. Experimental

In a typical procedure, appropriate amount of PVP was dissolved in 10 ml distilled water (with PVP to water weight ratio of 0% to 5%). Subsequently, 5 mM zinc acetate was added to the PVP solution under the stirring (500 rpm) and the resulting solution was homogenized for 30 min. Thereafter, 10 ml of the aqueous sulfur source solution was added and stirred until a well-dissolved solution was obtained. The final solutions were put in a high power microwave oven (1100 W) operated with a pulse regime of 20% power for 30 min. The precipitates were centrifuged and washed several times with distilled water and ethanol, then dried in the air at 60 ^{o}C for 24 h in a controlled environment.

The products were characterized by X-ray diffraction (XRD) at the scanning rate of 5^{o}/min in the 2θ range 20–70 ^{o} using a Philips X-ray diffractometer (7602 EA Almelo) with Cu Kα radiation (λ = 0.1542 nm). The morphology, particle size and size distribution were determined using the transmission electron microscopy (TEM) micrographs (HTACHI H-7100 TEM). The optical properties of ZnS nanoparticles were characterized using UV–visible absorption spectroscopy (UV-1650PC SHIMADZU) and photoluminescence (PL) spectroscopy (Perkin Elmer, LS-55: fluorescence spectrometer). The dielectric properties of the ZnS nanoparticles were measured using Precision LRC meter (Agilent-4284A) in the frequency range from 20 Hz to 1 MHz at room temperature. Samples were characterized in the shape of pellet with the dimension of 0.53 mm and 10.8 mm as thickness and diameter respectively.

3. Results and discussions

The formation of the PVP-capped ZnS nanoparticles can be observed by changing in the color of the solution from colorless to white and confirmed by powder X-ray diffraction studies. XRD patterns of ZnS nanoparticles obtained in the absence and presence of PVP are shown in Fig.1. For all samples, three diffraction crystalline planes of (111), (220) and (311) were observed in the XRD patterns and matched well with the cubic ZnS structure reported in ICDD PDF 80-0020. The lattice parameter of cubic nanocrystallines was calculated based on the X-ray diffraction patterns using [12]:

$$a^2 = d_{hkl}^2(h^2 + k^2 + l^2) \tag{1}$$

where a is the lattice parameter, h, k, and l are the Miller indices and d_{hkl} is the interplanar spacing corresponding to the Miller indices. The calculated values of the lattice constants and unit cell volumes are shown in Table 1. It can be seen that the values of lattice constant are in a good agreement with values reported in ICDD PDF 80-0020 (a = 5.34A^o).

Table 1. d-spacing, Lattice constant and unit cell volume of bare and PVP-capped ZnS nanoparticles

Sample	d_{hkl}–spacing (A^o)	Lattice constant a (A^o)	Unit cell volume (A^{o3})
Bare ZnS	3.095	5.36	154.05
PVP-ZnS (1%)	3.084	5.34	152.41
PVP-ZnS (3%)	3.079	5.33	151.42
PVP-ZnS (5%)	3.067	5.31	149.72

It is observed that in the presence of PVP, the intensity of XRD peaks for ZnS nanoparticles is lower than the peaks in the absence of the polymer. This trend is more pronounced when the concentration of PVP is increased, i.e. for higher percentage of PVP up to 5% the intensity of the peaks is lower. Moreover, all the peaks are slightly shifted towards higher 2θ values. These attribute to the lower degree of crystallinity and internal stress and strain [13], which strongly supports the formation of the PVP–capped ZnS nanoparticles.

The significance of the broadening peaks in the XRD spectra is due to the nanocrystalline nature of the samples. It also evidences the grain refinement along with the large strain associated with the nanoparticles [14]. From the width of the XRD peak, the mean crystalline size can be calculated using Debye-Scherrer's equation [15-16]:

$$D = \frac{k\lambda}{\beta \cos\theta} \tag{2}$$

where D is the average crystallite size, k is the particle shape factor that varies with the method of taking the breadth and shape of crystallites ($0.89<k<1$) [17], λ is the X-ray wavelength used (0.1542 nm), β is the angular line width of half-maximum intensity (FWHM) of the diffraction peak, and θ is the Bragg's angle in degrees. The average particle size calculated by the Debye-Scherrer's equation for the preferred plane (111) lies in the range of 4-6 nm (Table 2).

The strain (ε) induced in powders due to crystal imperfection and distortion can be calculated using Equation 3 [14]:

$$\varepsilon = \frac{\beta}{4\tan\theta} \tag{3}$$

Assuming that the particle size and strain contributions to the line broadening are independent from each other, the observed line breadth is simply the sum of the Equations 2 and 3 which results the Williamson-Hall equation:

$$\frac{\beta\cos\theta}{\lambda} = \frac{k}{D} + \frac{4\varepsilon\sin\theta}{\lambda} \tag{4}$$

This equation represents a straight line between $(4\sin\theta/\lambda)$ and $(\beta\cos\theta/\lambda)$. The slope of this line gives the strain, while the intercept (k/D) on y-axis gives the effective crystallite size (D) [12]. Fig. 2 shows the Williamson-Hall plots of the samples. The appearance of positive slopes

indicates the possibility of the tensile strain [18]. The calculated effective particle size shows slight variation with that of the results obtained by the Debye Scherrer's formula (see Table 2). The difference is due to the effects of internal strain, which is not considered in the Scherrer model.

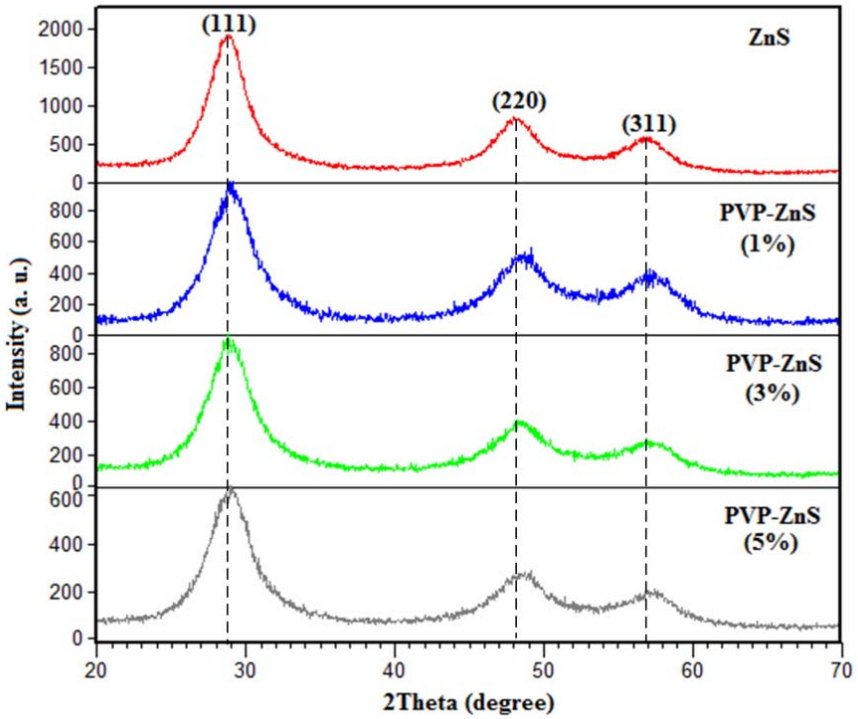

Fig 1. XRD patterns of bare and PVP-capped ZnS nanoparticles

Table 2. Crystallite size, strain and particle size of bare and PVP-capped ZnS nanoparticles

Sample	Average crystallite size by Scherrer's Formula (nm)	Effective crystallite size by Williamson-Hall plot (nm)	Strain ($\times 10^{-3}$)	Average particle size From TEM images (nm)
Bare ZnS	4.9	5.0	3.9	4.8
PVP-ZnS (1%)	4.8	5.2	9.5	5.3
PVP-ZnS (3%)	4.9	4.9	1.9	5.2
PVP-ZnS (5%)	4.4	4.6	3.4	5.1

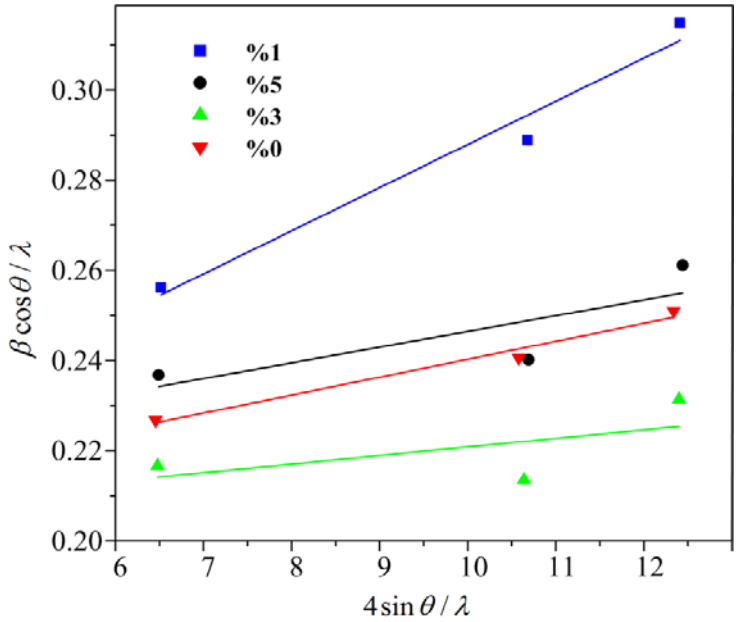

Fig 2. Williamson-Hall plots of bare and PVP-capped ZnS nanoparticles

TEM image of the pure zinc sulfide showed the formation of agglomerated nanoparticles. While after introducing appropriate amount of PVP, as it is shown in Fig. 3, the formation of spherical and homogeneous nanosize particles without any agglomerations was observed . In the absence of PVP, the CH_3COO^- anions bound to the surface of the ZnS nanoparticles and restrict the particle growth, whilst the hydrogen bonds between the CH_3COO^- anions promote aggregation [19]. After introducing PVP into the reaction mixture, the Zn^{2+} ions form a complex with PVP, which results in particle capping upon the nucleation, meanwhile the growth and agglomeration of the particles are increasingly controlled by the formation of passivation layers on the particles' surface. The average particle size obtained from the TEM images are listed in Table 2. It can be seen from the table that the particle sizes are in a fair agreement with those determined from XRD patterns.

The EDX and FTIR results are evidences for the formation of PVP passivation layers on the surface of particles. The EDX patterns of bare and PVP-capped (5%) ZnS nanoparticles are shown in Fig. 4 (a,b), and the related data are listed in Table 3. The peaks corresponding to the elements Zn and S were observed in the bare ZnS (Fig 4a) and the peaks of the elements Zn, S and O were observed in the PVP-capped ZnS nanoparticles (Fig 4b).

Table 3. EDX data of ZnS and PVP-capped ZnS nanoparticles (5%)

Sample	Wt% of Zn	Wt% of S	Wt% of other elements	At% of Zn	At% of S	At% of other elements
ZnS	69.37	30.63	0	52.63	47.37	0
PVP-ZnS	65.63	27.44	6.93	43.79	37.33	18.88

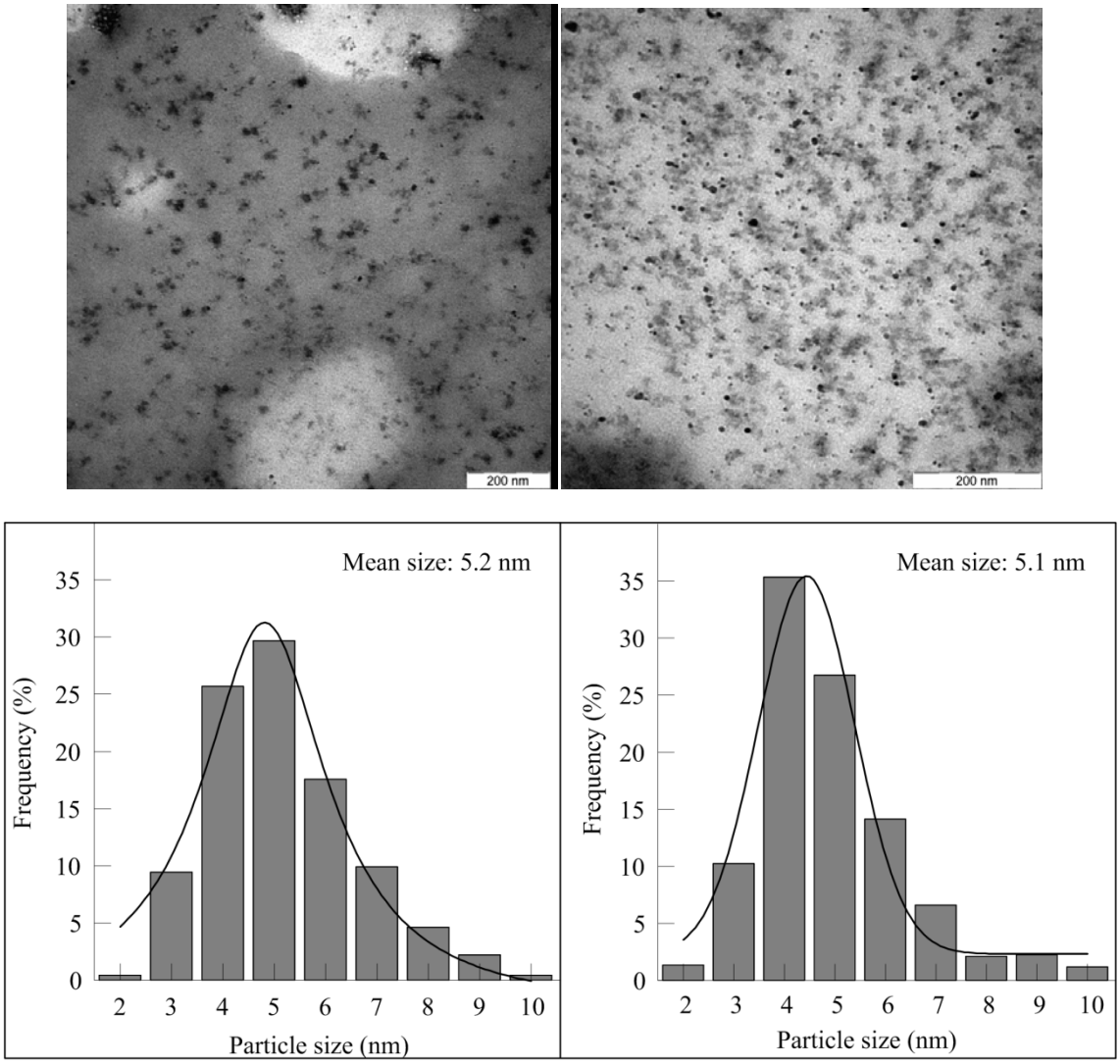

Fig 3. TEM image and particle size distribution histogram of PVP-capped ZnS nanoparticles 3% (left) and 5% (right)

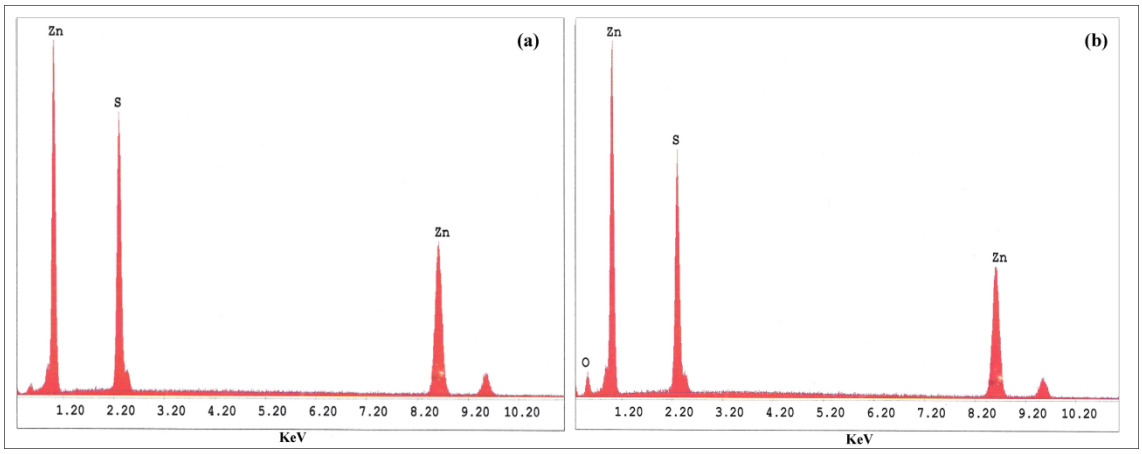

Fig 4. EDX patterns of (a) bare and (b) PVP-capped ZnS nanoparticles (5%)

For understanding the adsorption mechanism of PVP on the surface of nanoparticles, FTIR analysis of the PVP-capped ZnS nanoparticles were carried out and the obtained data were compared to the FTIR spectrum of the pure PVP. As it is shown in Fig 5, when the FTIR spectra of pure PVP and PVP-capped ZnS nanoparticles are compared, a prominent absorption peak at 1655 cm^{-1} (curve 'a') representing the functional C=O unit in PVP, shifts to 1635 cm^{-1} (curve 'b') and 1639 cm^{-1} (curve 'C') for the polymer concentration of 5 and 3%, respectively. Such a decrease in the wave number of C=O bond may occur due to the bond weakening as a result of the partial bond formation with the surface Zn atoms, which ultimately confirms the coordination of the ZnS nanoparticles with O atoms of C=O bonds of PVP. Furthermore, the other peaks of PVP, such as C–H and C-N, are significantly shifted or weakened that may be attributed to the production of shorter polymer chains during microwave irradiation.

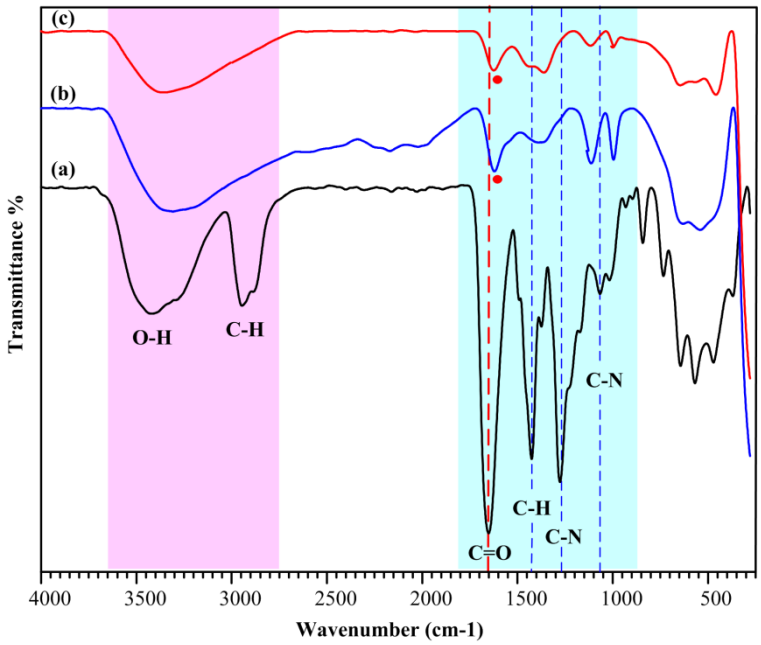

Fig 5. FTIR spectrum for (a) Pure PVP; (b) PVP-capped ZnS 5% and (c) PVP-capped ZnS 3%

The fundamental process of absorption or reflectance of the light by the semiconductor materials is relevant to their electronic structures. Hence, the UV-visible absorption studies play a vital role in estimating the optical band gaps using Tauc relation [20]:

$$\alpha h\nu = B(h\nu - E_g)^{1/2} \tag{5}$$

where α is the absorption coefficient, $h\nu$ is the photon energy, E_g is the direct band gap energy, and B is a constant. The band gap energy can be evaluated via a plot of $(h\nu\alpha)^2$ versus $(h\nu)$ and extrapolation of the linear portions of the curves to the energy axis. For different PVP concentrations of the PVP-capped ZnS nanoparticles, Fig. 6a and Fig. 6b demonstrate the results for UV–Visible absorption spectra and Tauc plots, respectively. The estimated optical band gaps of PVP-capped ZnS nanoparticles and the blue shift of absorption edges compared to the bulk counterpart are listed in Table 4.

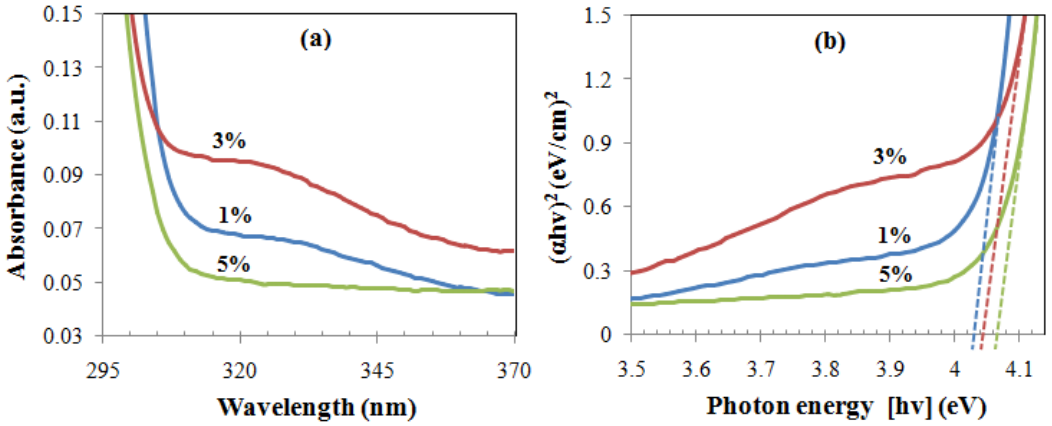

Fig 6. (a) UV–Vis absorption spectra and (b) Tauc plot of the PVP-capped ZnS nanoparticles.

From the band gap values, the particle sizes can be calculated using the Brus equation [21-22]:

$$\Delta E = \frac{\hbar^2 \pi^2}{2r^2}\left(\frac{1}{m_e^*} + \frac{1}{m_h^*}\right) - \frac{1.8e^2}{4\pi\varepsilon_0\varepsilon_r r} \tag{6}$$

where ΔE is the blue shift, m_e* and m_h* are the effective mass of the electron and hole, r is the particle radius, ε_r is the dielectric constant and ε_o is the permittivity of the free space.
From this equation, the particle sizes were calculated and listed in Table 4. It can be seen from the table that the particle sizes are in a fair agreement with those determined from the XRD patterns and TEM images.

Table 4. Optical band gap, blue shift and particle size of PVP-capped ZnS nanoparticles

Samples	Band gap (eV)	Blue shift (eV)	Particle Size (nm)
ZnS/PVP (1%)	4.03	0.35	5.2
ZnS/PVP (3%)	4.05	0.37	5.1
ZnS/PVP (5%)	4.07	0.39	5.0

Luminescence-based analytical techniques are very sensitive to detect discrete electronic states and can provide experimental evidence of electronic defects. On the surface of nanoparticles, the coordination number around the atoms is less than that inside the bulk. In this matter, there can be larger number of defect states which acts as non-radiative pathways for the excited electrons and becomes detrimental to the luminescent properties of the nanocrystalline phosphors. Therefore, modifying the nanoparticle surface using capping agents may passivate the defect states and dangling bond density, and change the PL intensity. Moreover, the excitation spectrum can be significantly modified due to the appearance of a set of new excitation bands [5].

The room temperature PL spectra of bare ZnS and PVP-capped ZnS nanoparticles under excitation wavelength of 270 nm are shown in Fig. 7. The PL spectra of the PVP capped ZnS nanoparticles appeared to be dramatically broadened from 370 to 500 nm due to the presence of multiple emission bands. Gaussian curve fitting was applied to de-convolute the multiple bands that constitute the envelope spectrum. The broadened PL spectra of samples have been de-

convoluted into three different bands with the peak maxima at 420, 460 and 480 nm. The first and third peaks attribute to the recombination of electron-hole pairs in sulfur and zinc vacancies of ZnS nanoparticles. These two individual components were clearly observed in PL spectra of the bare ZnS nanoparticles. The second peak is assumed to originate from the radiative recombination of carriers at the surface trap states resulted from the compounded effect of PVP. Since the emission characteristics of the ZnS nanoparticles depend on the concentration of vacancy centers [5], the relative intensities of bands vary with the change in the concentration of PVP. As it can be seen in Fig. 7, by incresing the PVP concentration the intensity of the peaks is decreased, which is probably related to decrease in the degree of crystallinity and increase of the crystal defects.

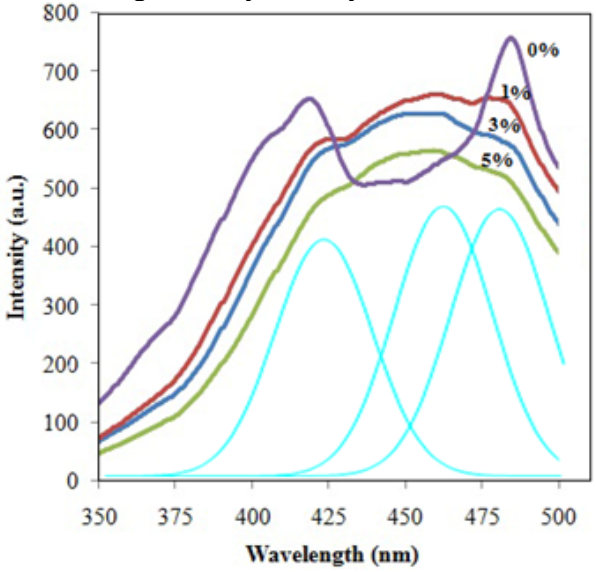

Fig 7. Photoluminescence spectra of bare and PVP-capped ZnS nanoparticles recorded at an excitation wavelength of 270 nm

Fig. 8 shows the frequency variation of conductivity σ (ω) for the ZnS nanoparticles prepared in different PVP concentration. The direct extrapolated DC conductivity (σ_{dc} (ω)) showed the value of 2.981×10^{-6}, 5.194×10^{-6} and 7.014×10^{-6} S/m for 1, 3 and 5% PVP concentration respectively, which indicates conductivity enhancement by increasing the PVP concentration. The value of σ_{dc} (ω) increases by raising the PVP concentration. This increament can be due to the presence of few free charges originated from the crystal defects, which provides a slight motion to present the small DC behaviour.

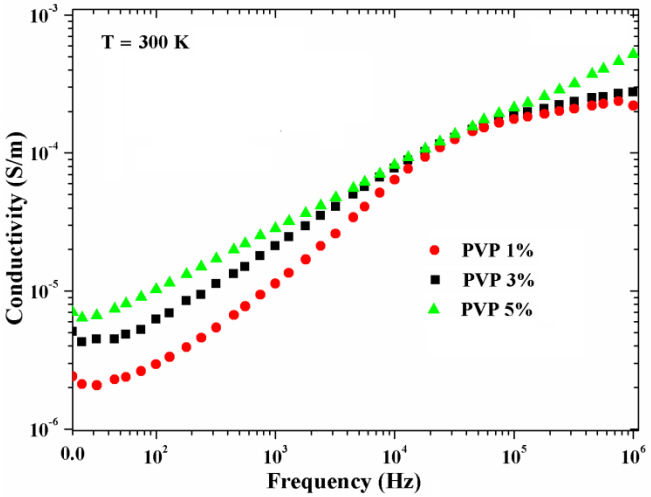

Fig 8. variation of general conductivity with frequency for the PVP-capped ZnS nanoparticles

However, the variation of σ (ω) indicates the overal AC behaviour. As the FTIR graph indicates, whenever the PVP concentration increases the presence of the PVP as a shell increases, which leads to have more traps in polymer shells. Moreover, the photo luninecence graph illustrates that the crystal defects are increased by raising the PVP concentration. According to the presence of these trapped ions (crystal defects), conductivity values in Fig.8 show more AC behavior than DC behavior which is basically related to the free carriers to conduct the DC current.

The impedance of ZnS nanoparticles prepared at different PVP concentrations were measured at room temperature under zero bias with an applied small signal voltage in the frequency range of 20 Hz to1MHz. In order to find the DC conductivity, the Niquist diagram is plotted (Fig. 9) and Z_0 (resistance at zero frequency) is extracted from the intercept for the best fitting experimental points, when Z" = 0 (the Z' and Z" values shown in Fig. 9 are real and imaginary part of total impedance, respectively). The complex impedance plot shown in Fig. 9 is modeled by Cole-Cole modification of the Debye equation [23]. The DC conductivity (σ_{dc} (ω)) can be calculated for samples with PVP concentrations of 1 and 3%, which are 3.07×10^{-6} and 5.26×10^{-6} S/m, respectively. These values are in the range of insulators and in a good agreement with extrapolated values from Fig. 8.

As it is mentioned before, the behavior of the PVP-capped ZnS nanoparticles is AC conductivity, due to the presence of polymer and crystal defects in the structure. However, a small value of DC conductivity originated from low numbers of free charges, can be obtained for samples with 1 and 3% of PVP concentration. Eventually, for the sample with the highest PVP concentration (5%), nearly all free charges or ions were trapped and no DC behavior was observed, as it can be seen in Fig. 9.

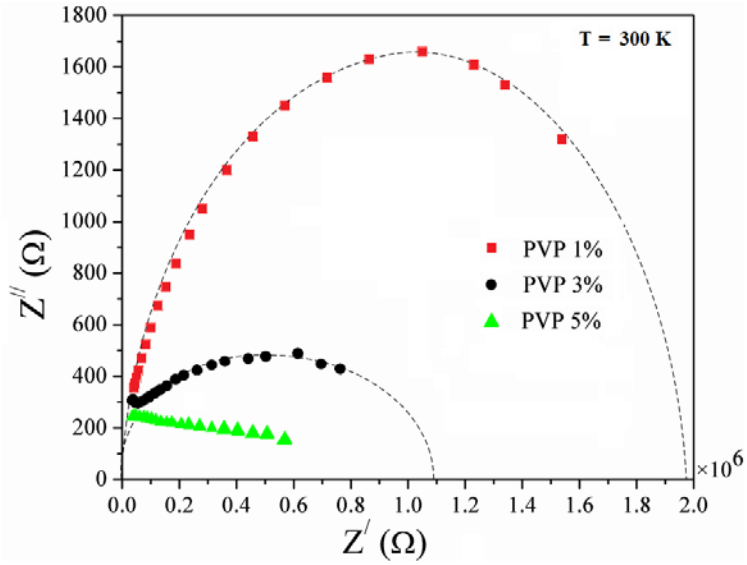

Fig 9. Niquist diagram of PVP-capped ZnS nanoparticles

Basically, when a time-dependent field is applied to the dielectric or semiconductor materials, the polarization process is time-dependent as well [24]. However, due to the presence of the resistance against the motion of the atoms through the material, there is a phase delay between changes in the field and polarization. This phase difference is mostly stated as a loss angle (δ), which also expressed as the dissipation factor or tan δ. The energy absorbed from the time-dependent field by the dielectric material per cycle, is directly proportional to the loss factor from the time-dependent field [25]. In crystalline defects, the charge carriers, such as free charges, cavities and polar groups can affect the dielectric constant [26].

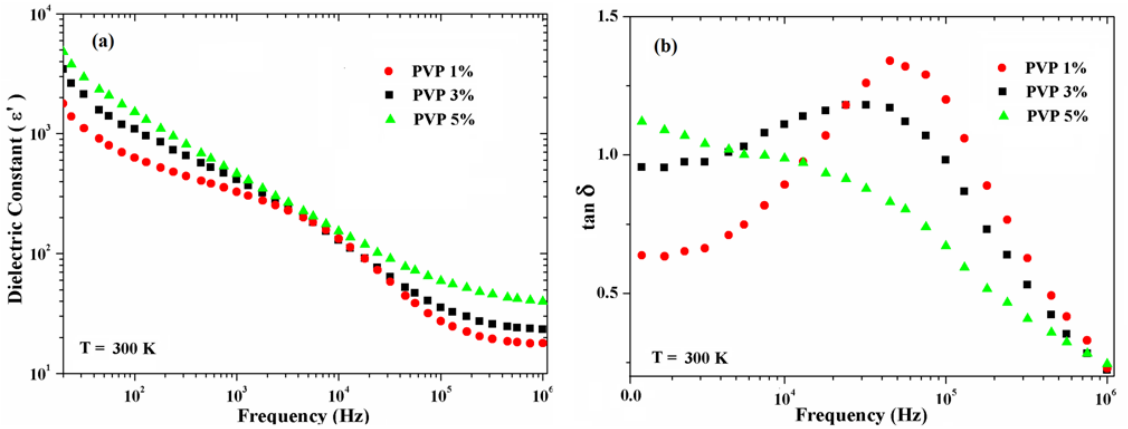

Fig 10. Variation of dielectric constant (a) and tan δ (b) with frequency of PVP-capped ZnS nanoparticles

The variation of the frequency with dielectric constant ($\mathcal{E}$') and dissipation factor (tan δ) at room temperatures for ZnS nanoparticles, prepared at different PVP concentrations, are shown in Fig. 10 (a,b). For all samples, a relaxation is observed as a gradual decrease in dielectric constant ($\mathcal{E}$') with increasing frequency (Fig. 10a). For low frequencies, dipoles in atomic structure are still able to follow the external field oscillation. However, for high range of frequency (after 10^5 Hz in our case), these dipoles begin to fall behind the external field and the value of $\mathcal{E}$' tends to change slightly, which indicates the saturation state of polarization [27]. Similar behavior for ZnS nanoparticles prepared by different method was reported previously [11]. The $\mathcal{E}$' values are increasing by raising the PVP concentration, whereas it decreases with increasing the frequency. The increament of the PVP concentration during ZnS nanoparticles preparation, in addition to the presence of crystal defects, lead to have more polar centeres in the structure as well as increasing the dielectric constant.

Fig. 10b shows the existence of a peak in the tan δ values for the PVP-capped ZnS nanoparticles, especially for the sample prepared at lowest rate of PVP concentration (1%). This peak tends to be decreased for the higher rate of PVP concentration, while it is disappeared for the sample prepared at the highest rate (5%). The decrease in the peak value of tan δ with the increase of PVP concentration indicates the reduction of the charge carriers in these samples, as mentioned earlier. It is found that the tan δ values of the nanoparticles prepared at 5% PVP concentration decreases at higher frequency ranges (after 10^4 Hz). This can be explained due to the low numbers of charge carriers (lack of the free charge motion) in this particular sample which leads to decrease in the dielectric loss value [27] .

4. Conclusions

A simple microwave irradiation method was used for the synthesis of PVP-capped ZnS nanoparticles. Differences in the structural, optical and electrical properties of ZnS nanoparticles were found to be polymer concentration dependent as visible upon XRD, TEM, UV-visible and PL spectra and LRC meter measurements. Capping with PVP occurred via conjugation between C=O band of PVP and the ZnS nanoparticles as confirmed via FTIR analysis. The potential of capping ZnS nanoparticles is illustrated by the fact that PVP-capped ZnS nanoparticles exhibit some measure of control over the size, structure and especially optical and electrical properties of the material.

References

[1] Y. Ni, G. Yin, J. Hong and Z. Xu, Mater. Res. Bull. **39,** 1967 (2004).
[2] S. Mondal, H. Mullick, T. Lavanya, A. Dhar, S. Ray and S. Lahiri, J.Appl. Phys. **102**, 064305 (2007).

[3] R. Seoudi, A. Shabaka, W.H. Eisa, B. Anies and N.M. Farage, Physica B. **405**, 919 (2010).
[4] A. Khare, J. Phys. Chem. Solid. **73**, 839 (2012).
[5] K. Manzoor, S.R. Vadera, N. Kumar and T.R.N. Kutty, Solid. State. Commun. **129**, 469 (2004).
[6] D.C. Onwudiwe and P.A. Ajibade, Int. J. Mol. Sci. **12**, 5538 (2011).
[7] R. He, X.-f. Qian, J. Yin, H.-a. Xi, L.-j. Bian and Z.-k. Zhu, Colloid. Surface. A. **220**, 151 (2003).
[8] N. Tomczak, D. Janczewski, M. Han and G.J. Vancso, Prog. Polym. Sci. **34**, 393 (2009).
[9] S.-Z. Kang, Y. Yang, Z. Xu and J. Mu, J. Disper. Sci. Technol. **29**, 521 (2008).
[10] P. Verma, G.S. Manoj and A.C. Pandey, Physica B. **405**, 1253 (2010).
[11] N. Soltani, A. Dehzangi, E. Saion, M.Y. Majlis, M.R. Zare, A. Kharazmi and M. Navasery, Chalcogenide. Letters. **10**, 27 (2013).
[12] G. Theophil Anand, L. John Kennedy and J. Judith Vijaya, J. Alloy. Compd. **581**, 558 (2013).
[13] M. Navasery, S. Halim, K. Lim, S. Chen, A. Roslan and R. Abd-Shukor, Mod. Phys. Let. B. **26**, 50039 (2012).
[14] V. Mote, Y. Purushotham and B. Dole, J. Theor. Appl. Phys. **6**, 1 (2012).
[15] J. Li, Y. Xu, Y. Liu, D. Wu and Y. Sun, China. Particuology. **2**, 266 (2004).
[16] M.A. Behnajady, N. Modirshahla and E. Ghazalian, Digest. J. Nanomater. Biostructure. **6**, 467 (2011).
[17] S. Singh, H. Kaur, D. Pathak and R.K. Bedi, Digest. J. Nanomater. and Biostructure. **6**, 689 (2011).
[18] A. Maurya, P. Chauhan, S.K. Mishra and R.K. Srivastava, J. Alloy. Compd. **509**, 8433 (2011).
[19] Q.-Z. Yao, G. Jin and G.-T. Zhou, Mater. Chem. Phys. **109**, 164 (2008).
[20] R. Seoudi, A. Shabaka, W.H. Eisa, B. Anies and N.M. Farage, Physica B. **405**, 919 (2010).
[21] S. Phoka, P. Laokul, E. Swatsitang, V. Promarak, S. Seraphin and S. Maensiri, Mater. Chem. Phys. **115**, 423 (2009).
[22] M. Pattabi, B. Saraswathi Amma, K. Manzoor and S. Ganesh, Sol. Energ. Mat. Sol. C. **91**, 1403 (2007).
[23] K.S. Cole and R.H. Cole, J. Chem. Phys. **9**, 341 (1941).
[24] C. Kittel and P. McEuen, *Introduction to solid state physics*. Vol. 7. 1996: Wiley New York.
[25] R. Tripathi, A. Kumar and T.P. Sinha, Pramana. **72**, 969 (2009).
[26] W. Wan, D. Yu, Y. Xie, X. Guo, Z. Mao and L. Huang. in *Nano/Micro Engineered and Molecular Systems, 2006. NEMS'06. 1st IEEE International Conference* (2006).
[27] P. Dutta, S. Biswas and S.K. De, Mater. Res. Bull. **37**, 193 (2002).